

“Striped” Rectangular Rigid Box with Hermitian and non-Hermitian \mathcal{PT} Symmetric Potentials

Shailesh Kulkarni* and Rajeev K. Pathak†

Department of Physics, Savitribai Phule Pune University, Ganeshkhind, Pune, 411007, India

ABSTRACT

Eigenspectra of a spinless quantum particle trapped inside a rigid, rectangular, two-dimensional (2D) box subject to diverse inner potential distributions are investigated under hermitian, as well as non-hermitian antiunitary \mathcal{PT} (composite parity and time-reversal) symmetric regimes. Four sectors or “stripes” inscribed in the rigid box comprising contiguously conjoined parallel rectangular segments with one side equaling the entire width of the box are studied. The stripes encompass piecewise constant potentials whose exact, complete energy eigenspectrum is obtained employing matrix mechanics. Various striped potential compositions, viz. real valued ones in the hermitian regime as well as complex, non-hermitian but \mathcal{PT} symmetric ones are considered separately and in conjunction, unraveling among typical lowest lying eigenvalues, retention and breakdown scenarios engendered by the \mathcal{PT} symmetry, bearing upon the strength of non-hermitian sectors. Some states exhibit a remarkable crossover of symmetry ‘making’ and ‘breaking’: while a broken \mathcal{PT} gets reinstated for an energy level, *higher* levels may couple to continue with symmetry breaking. Further, for a charged quantum particle a \mathcal{PT} symmetric electric field, furnished with a striped potential backdrop, also reveals peculiar retention and breakdown \mathcal{PT} scenarios. Depictions of prominent probability redistributions relating to various potential distributions both under norm conserving unitary regime for hermitian Hamiltonians and non-conserving ones post \mathcal{PT} breakdown are presented.

*e-mail : shailesh@physics.unipune.ac.in

†e-mail : snehalandrajeev@gmail.com

1 Introduction

Among the few problems that pragmatically merit exact quantum mechanical solutions, the ‘rigid-box’ problems form a special class signifying, contingent on dimensionality and symmetry, a quantum particle confined within some standard geometries such as line segments, rectangular and circular areas, rectangular parallelepipeds (cuboids), cubes, spheroids, spheres and thus forth. In all these cases, as is well-known, appropriately chosen coordinate systems permit separation of variables in the configuration space, yielding analytical solutions. Following its inception by McDonald and Kaufman [1], ‘Quantum Billiards’ (QB), that has emerged a generic term for analyzing the dynamics of a particle in confined spaces, has stimulated widespread interest over the past four decades [2–8]. Although even a slightest deviation from standard shapes could render a systematically tractable solution impossible, cogent numerical methods to tackle such situations have been developed [9, 10]. Interestingly, particles moving in polygonal enclosures whose interior angles are rational multiples of π were observed to exhibit ‘pseudo-integrability’ embodying tenets of quantum chaos [11]. Moreover, some customized mesoscopic semiconductor quantum dots were experimentally observed to exhibit salient QB characteristics in terms of forward and back-scattered electron wave-packets and their revivals [12]. Later, a case strikingly akin to this effect was impeccably solved *exactly* by Robinett [5], for a 2D rigid circular box augmented by an infinite thin barrier or baffle introduced along one of its radii constituting quantum billiards. Noticeably, QB were demonstrated to furnish a manifest natural connection between the complementary phenomena of classical and quantum chaos [2, 3].

Meanwhile, Bender and Boettcher [14], through their pioneering article in 1998, launched the exotic theme of \mathcal{PT} Symmetry, signifying invariance of the Hamiltonian under the composite, discrete symmetry operations of Parity (\mathcal{P}) and Time-reversal (\mathcal{T}), irrespective of their order of application, for a wide variety of systems. Introduction of \mathcal{PT} symmetry, a remarkable non-Hermitian extension of Quantum Mechanics, has evoked inexorable intrigue and has stimulated a multitude of theoretical [14, 15] as well as experimental [16, 17] ventures. When in a Hamiltonian system, a perfect balance is struck between gain and loss mechanisms, \mathcal{PT} symmetry manifests through the corresponding potential (energy) terms. \mathcal{PT} symmetry also got introduced in confined quantum systems by several workers: notably, Bittner *et al.* [18] examined a two-state Hamiltonian of a dissipative microwave billiard in the neighborhood of an exceptional point, bringing forth a peculiar \mathcal{PT} symmetry. Further, Dasarathy *et al.* [19] imposed \mathcal{PT} symmetry not by parameterizing the Hamiltonian, but rather implicitly, through the *boundary conditions* over

the standard 1D rigid box segment and established that the ensuing dynamics invariably conformed to a robust \mathcal{PT} symmetry. In their recent experiments, Gu and coworkers [20] ingeniously demonstrated incorporation of \mathcal{PT} symmetry in a “Stripe-LASER” waveguide with its pumped part functioning as ‘gain’, and the other unpumped one serving as ‘loss’, due to the intrinsic absorption of a deliberately introduced dye. Interestingly, Kreibich [21] presented a concrete scenario for realizing \mathcal{PT} symmetry for particle currents in Bose-Einstein condensates, simulating a two-mode model system embedded in a larger *hermitian* system having at least four additional coupled ‘reservoir’ wells equipped with a balanced gain-loss mechanism. For discrete confined systems, Musslimani *et al.* [22] conclusively demonstrated that \mathcal{PT} symmetry can support soliton solutions in 1D as well as 2D nonlinear optical lattices. \mathcal{PT} symmetry thus is not limited to a theoretical abstraction, but also presents tangible perspectives amenable to direct experimentation [15–17].

Induction of \mathcal{PT} symmetry in the ‘particle-in-a-box’ context was likewise carried out, in particular, by Yusupov *et al.* [23], who studied the quantum dynamics in a 1D box, driven by a \mathcal{PT} symmetric complex potential, with impulsive, non-Hermitian, delta-function ‘kicks’, and observed that the otherwise sustained \mathcal{PT} symmetry broke down beyond certain characteristic threshold strengths of the kicking parameter. Interestingly, notwithstanding the standard constraints for the elementary 1D rigid box problem, Adamu [24], by a direct *post facto* imposition of the \mathcal{PT} symmetric *boundary conditions* on the eigenfunctions, obtained a distinct class of eigenfunctions associated with the same eigenvalues as that of the usual 1D box. Around the same time, Fernández and Garcia [25] applied perturbation theory to a 2D rigid square box incorporating some model parameterized \mathcal{PT} symmetric potentials, that exhibited retention of \mathcal{PT} symmetry below some specific threshold parameter-values.

For yet another confined 2D system albeit with circular geometry, Agarwal and others [26] presented exact solutions to typified \mathcal{PT} symmetric potentials with sinusoidally oscillating azimuth, revealing some counterintuitive \mathcal{PT} breakdown scenarios, e.g. raising the hermitian component sometimes resulted in accelerating, rather than deterring, breaching of \mathcal{PT} . Further, in another exploration on \mathcal{PT} applied to 2D, finite *discrete* latticework, these workers [27] demonstrated that for a set of coupled chains in 2D with only two balanced gain-loss \mathcal{PT} sites interspersed, the transition threshold could be markedly enhanced as a function of the coupling, providing a handle on tune-ability. Incidentally, for a 1D rigid box, a family of \mathcal{PT} symmetric complex potentials isospectral with its eigenspectrum was obtained [28].

The foregoing discussion emphasizes that quantum particles in entrenched, or con-

fined, quantum billiards type configurations could exhibit uncommon dynamics, accentuated with application of \mathcal{PT} symmetry. Subscribing to this premise, the present article is aimed at systematically studying the behavior of a spinless particle in a ‘striped’ two dimensional rectangular rigid quantum box, a special type of quantum billiards whose *exact* quantum mechanical energy eigenspectrum will be obtained. Piecewise constant potentials are introduced along the breadth of the box, in chosen sectors or stripes, where some or all of them are selectively rendered hermitian and/or \mathcal{PT} symmetric, the latter accomplished by introduction of balanced gain and loss sectors. We delineate onset of \mathcal{PT} symmetry breaking at characteristic exceptional points and bring forth the consequent mutations in the probability density. While the present venture evidently provides *exact* solutions to a model quantum mechanical situation, a pertinent physical problem that could serve as its excellent prototype would be a three dimensional tubular wave-guide with a uniform rectangular normal cross-section, with propagation of the particle or light flux in the longitudinal positive z direction, and a suitably tune-able lateral beam distribution in the $x - y$ plane: for a 1D analogue, reference may be made to the work of Moiseyev and others [29], who studied a waveguide with a piecewise constant *complex* refractive indices. In the present problem, preemptively factoring out the plane-wave propagation along positive z , we focus on the wave function projected onto the plane, within the ambit of the rectangle. It will turn out that the exactly solvable 2D rectangular rigid box, in conjunction with a stipulated \mathcal{PT} symmetric potential distribution in the interior also selectively exhibits sustenance and abrogation of the symmetry consequent to the interplay between the relative strengths of the intervening potentials.

2 Two dimensional rectangular rigid box with striped potential distribution: exact solutions

We consider a rigid rectangular box in the Cartesian $x - y$ plane, bounded by $0 \leq x \leq a, 0 \leq y \leq b$, partitioned with piecewise constant potentials V_1, V_2, V_3 and V_4 in contiguous rectangular sectors or stripes throughout their breadth, equaling the breadth of the rigid box, parallel to the x -axis. The inside potentials are finite with possible finite discontinuities at each interface within the box. The rectangular sectors, i.e. the stripes are symmetric around the y -median as depicted in the accompanying schematic Figure-1. The region outside the box, of course, is impenetrable, with positive infinite potential.

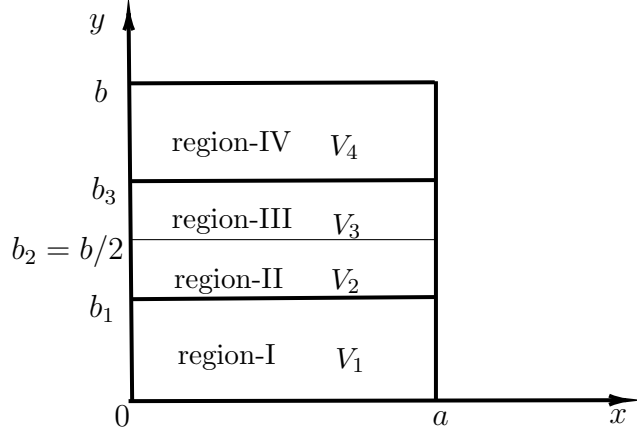


Figure 1: A schematic “striped” rectangular box in the $x - y$ plane, with $0 < x < a, 0 < y < b$; partitioned with four rectangular sectors I, II, III and IV respectively bearing the piecewise constant, finite potentials V_1, V_2, V_3 and V_4 . The partitions are symmetric with respect to the median $y = b/2 \equiv b_2$, whence, $b_3 - b_2 = b_2 - b_1 < b/2$. Outside the box, throughout, the potential is $+\infty$.

The potential $V(x, y)$ within the rigid box is designated as follows:

$$V(x, y) = \begin{cases} V_4, & b_3 < y < b \\ V_3, & b_2 < y < b_3 \\ V_2, & b_1 < y < b_2 \\ V_1, & 0 < y < b_1 \end{cases}$$

with $0 < x < a$ throughout and $V(x, y) \rightarrow +\infty$, outside the rectangle. Note that within the box, the only explicit dependence of the potential $V(x, y)$ is on the y -coordinate; therefore inside, $V(x, y) \equiv V(y)$ alone, a fact that will be exploited shortly. The stationary states for a scalar (spinless) particle of mass μ trapped inside the planar 2D rectangular geometry are the solutions of the time-independent Schrödinger equation

$$\hat{H}\psi(x, y) \equiv -\frac{\hbar^2}{2\mu} [\nabla_{2D}^2 + V(x, y)]\psi(x, y) = E\psi(x, y) \quad (1)$$

where ∇_{2D}^2 is 2D Laplacian operator and $\psi(x, y)$ designating the time-independent energy eigenfunctions associated with energy eigenvalues E of the Hamiltonian operator \hat{H} . Let us recall that for the standard, rudimentary text book case of a particle entrapped in the rigid box, but otherwise free inside, i.e. $V(x, y) = 0$ throughout the box, the corresponding eigenfunctions $\psi_{n_x, n_y}^{(0)}(x, y)$ factorize themselves as $\psi_{n_x, n_y}^{(0)}(x, y) = u_{n_x}(x)u_{n_y}(y)$ within the box and identically vanish outside the rectangle. The quantum numbers n_x and n_y take values $1, 2, \dots$. The normalized forms of the factor functions are

$$u_{n_x}(x) = \begin{cases} \sqrt{\frac{2}{a}} \sin\left(\frac{n_x \pi x}{a}\right), & 0 \leq x \leq a \\ 0, & \text{otherwise} \end{cases}$$

and

$$u_{n_y}(y) = \begin{cases} \sqrt{\frac{2}{b}} \sin\left(\frac{n_y \pi y}{b}\right), & 0 \leq y \leq b \\ 0, & \text{otherwise} \end{cases}$$

while the energy eigenvalues emerge as

$$E_{n_x, n_y}^{(0)} = \frac{\pi^2 \hbar^2}{2\mu} \left(\frac{n_x^2}{a^2} + \frac{n_y^2}{b^2} \right)$$

Note that degeneracies, including accidental degeneracies, could occur in this bound state two dimensional (2D) problem. To solve for the eigenspectrum of the striped box, we expand the wave function $\Psi(x, y)$ *vide* the completeness of the product functions $u_{n_x}(x)u_{n_y}(y)$:

$$\psi(x, y) = \sum_{n_x, n_y=1}^{\infty} C_{n_x, n_y} u_{n_x}(x) u_{n_y}(y) \quad (2)$$

Substituting the above in Eq. (1), one is led to

$$\sum_{n_x=1}^{\infty} u_{n_x}(x) \sum_{n_y=1}^{\infty} \left[\frac{\pi^2 \hbar^2}{2\mu} \left(\frac{n_x^2}{a^2} + \frac{n_y^2}{b^2} \right) + V(y) \right] C_{n_x, n_y} u_{n_y}(y) = E \sum_{n_x=1}^{\infty} u_{n_x}(x) \sum_{n_y=1}^{\infty} C_{n_x, n_y} u_{n_y}(y); \quad (3)$$

owing to the explicit dependence of the potential exclusively on the y -coordinate, within the rectangle. This leads to the separation of the x -solution altogether, whence, exploiting the linear independence of the functions $\{u_{n_x}(x)\}$ one arrives at

$$\sum_{n_y=1}^{\infty} \left[\frac{\pi^2 \hbar^2}{2\mu} \left(\frac{n_x^2}{a^2} + \frac{n_y^2}{b^2} \right) + V(y) - E \right] C_{n_x, n_y} u_{n_y}(y) = 0. \quad (4)$$

Since the x -dependence separates out (analogous to that coordinate being ‘‘cyclic’’ in the Hamiltonian defined over the box-region), we can designate the n_x quantum number a definite, fixed value, say $n_x \equiv n_x^{(0)}$ for the x -solution, which is then denoted by $u_{n_x^{(0)}}(x)$. Next, we substitute the appropriate piecewise constant forms for $V(y)$ in the four sectors, clamp the n_x quantum number at the chosen $n_x^{(0)}$ value, pre-multiply the above Eq. (4) throughout by $u_{n_y'}^*(y)$ and integrate over the y in the domain $[0, b]$. Implementing this in sequential conjunction and harnessing the orthonormality of $u_{n_y}(x)$ functions the procedure results in the following connection:

$$\sum_{n_y=1}^{\infty} \left\{ \frac{\pi^2 \hbar^2}{2\mu} \left[\frac{(n_x^{(0)})^2}{a^2} + \frac{n_y^2}{b^2} \right] - E \right\} C_{n_y}^{n_x^{(0)}} \delta_{n_y', n_y} + \frac{2}{b} \sum_{n_y=1}^{\infty} \left(\sum_{i=1}^4 V_i \int_{b_{i-1}}^{b_i} dy \phi(y) \right) C_{n_y}^{n_x^{(0)}} = 0 \quad (5)$$

where $b_0 \equiv 0$ and $b_4 \equiv b$ and $\phi(y) = \sin\left(\frac{n_y' \pi y}{b}\right) \sin\left(\frac{n_y \pi y}{b}\right)$. The coefficients have been relabeled as $C_{n_x^{(0)}, n_y}^{(0)} \equiv C_{n_y}^{n_x^{(0)}}$, reminding that only the discrete index n_y actually varies,

the index $n_x^{(0)}$ having been clamped. The wave function then simplifies to

$$\psi(x, y) = u_{n_x^{(0)}}(x) \sum_{n_y=1}^{\infty} C_{n_y}^{n_x^{(0)}} u_{n_y}(y) \quad (6)$$

After evaluation of the integrals the above line of arguments engenders a matrix eigenvalue equation

$$[M][C] = E[C]. \quad (7)$$

Here, the matrix $M = [M]_{n'_y, n_y}$ is an infinite dimensional ‘square’ matrix, labeled by the respective row and column indices $n'_y, n_y = 1, 2, 3 \dots$; while $C_{n_y}^{n_x^{(0)}}$ incarnates as a column vector. The matrix elements of M bear the explicit form

$$\begin{aligned} M_{n_y, n_y} &= \left[\frac{\pi^2 \hbar^2}{2\mu} \left(\frac{(n_x^{(0)})^2}{a^2} + \frac{n_y^2}{b^2} \right) \right] + \frac{1}{b} \sum_{i=1}^3 b_i (V_i - V_{i+1}) + V_4 \\ &+ \frac{1}{2\pi n_y} \left[\sum_{i=1}^3 (V_{i+1} - V_i) \sin \left(\frac{2\pi n_y b_i}{b} \right) \right]; \end{aligned} \quad (8)$$

for the diagonal entries, and

$$\begin{aligned} M_{n'_y, n_y} &= \frac{1}{\pi(n'_y - n_y)} \left[\sum_{i=1}^3 (V_i - V_{i+1}) \sin \left(\frac{\pi(n'_y - n_y) b_i}{b} \right) \right] \\ &+ \frac{1}{\pi(n'_y + n_y)} \left[\sum_{i=1}^3 (V_{i+1} - V_i) \sin \left(\frac{\pi(n'_y + n_y) b_i}{b} \right) \right]; \end{aligned} \quad (9)$$

for the off-diagonal entries ($n'_y \neq n_y$). We shall put the foregoing analysis to test with a variegated set of hermitian, and non-hermitian but \mathcal{PT} symmetric combinations, as carried out in the next section.

3 Results and discussion

To tackle the stationary-state problem for seeking the eigenvalues and eigenfunctions, we must adopt an appropriate scale. Setting the Bohr radius $a_B \equiv \frac{4\pi\epsilon_0 \hbar^2}{m_e e^2}$ (in usual notation) to represent a unit distance, and \hbar and the electron mass, m_e both numerically unity, the energy scale is set by the quantity $\frac{\hbar^2}{2m_e a_B^2} = 13.605693 \text{ eV} \equiv 1 \text{ Rydberg energy}$. Thus, we shall measure distances in units of Bohr radii and energies in units of Rydbergs. We also have, for convenience (although not direly necessary), chosen the mass of the quantum particle μ to be the electron mass, m_e . The task now is to solve the matrix equation,

Eq. (7), with the prescriptions in Eqs. (8) and (9) above. For nontrivial solutions, the secular equation, viz. $\det[M - EI] = 0$ (with I denoting the identity matrix) must be satisfied, which determines the energy eigenvalues E and thereafter, corresponding to each eigenvalue, the column vector C formed of the expansion coefficients, readily synthesizes the wave function as stipulated by Eq. (6).

Although in principle, the range spanned by the quantum numbers n'_y, n_y goes from 1 to ∞ , in practice, a proper upper limit n_y^{max} must be chosen for numerical implementation of the exact matrix-eigenvalue-equation, Eq.(7). It turns out that for an accurate evaluation the lowest 15-odd energy eigenvalues for maximal magnitude of the V_i (cf. Figure-1) 150 Ry energy units, the upper limit of $n_y^{max} = 30$ suffices for convergence to occur. We have chosen a better stringent and robust upper limit of $n_y^{max} = 50$, for reaffirming convergence of the lowest eigenvalues, rendering the computations numerically completely unequivocal. The convergence is markedly rapid, which may be attributed to the following: for sufficiently large values of n'_y and n_y , the diagonal elements of the Matrix M , (cf. Eq.(8)) form the major contribution, as they scale as $\sim (n'_y)^2$, while the off-diagonal ones far removed from the principal diagonal, scale magnitude wise as $\sim 1/n'_y$ or $\sim 1/n_y$ (cf. Eq.(9)), endowing a relative significance of $\sim (n'_y)^3$ to the diagonal elements over the far off-diagonals, thereby imparting a desirable characteristic for convergence.

If the origin is chosen to be the center of inversion, the parity operator \mathcal{P} , which is a linear and hermitian transformation maps a generic wave function $\psi(\vec{r}, t)$ in accord with $\mathcal{P}\psi(\vec{r}, t) = \psi(-\vec{r}, t)$ whereas the antilinear time-reversal \mathcal{T} transformation accomplishes the mapping $\mathcal{T}\psi(\vec{r}, t) = \psi^*(\vec{r}, -t)$. Further, since $\mathcal{P} = \mathcal{P}^{-1}$, for the present *spinless* case, $\mathcal{T} = \mathcal{T}^{-1}$ (while incidentally, for half-odd-integral spins, due to Kramers's degeneracy, $\mathcal{T}^2 = -I$, the negative identity), in the coordinate representation for the position and canonical momentum operators respectively follow the operator identities:

$$\mathcal{P} \vec{r} \mathcal{P}^{-1} = -\vec{r}, \quad \mathcal{T} \vec{r} \mathcal{T}^{-1} = \vec{r}, \quad \mathcal{P} \hat{p} \mathcal{P}^{-1} = -\hat{p}, \quad \mathcal{T} \hat{p} \mathcal{T}^{-1} = -\hat{p}$$

Further $[\mathcal{P}, \mathcal{T}] = 0$, and \hat{H} is said to be \mathcal{PT} symmetric if $[\hat{H}, \mathcal{PT}] = 0$. This requires that for the single spinless particle [21] :

$$(\mathcal{PT})\hat{H} = \left[\frac{(\hat{p})^2}{2\mu} + V^*(-\vec{r}) \right] \mathcal{PT} = \hat{H}(\mathcal{PT}), \quad (10)$$

since the antilinear T symmetry deems the transformation for a general complex-valued, explicitly time independent potential V , as $V \equiv Re(V) + i Im(V) \rightarrow Re(V) - i Im(V) = V^*$. Further, for an eigenstate $|\psi\rangle$,

$$\hat{H}|\psi\rangle = E|\psi\rangle \implies \hat{H} \mathcal{PT} |\psi\rangle = E^* \mathcal{PT} |\psi\rangle; \quad (11)$$

thus retention of \mathcal{PT} symmetry manifests in reality of the eigenvalues, while post- \mathcal{PT} breakdown, energy eigenvalues must occur in complex conjugate-pairs. \mathcal{PT} symmetry is still intriguing, since, especially for a multivariate problem, it is indiscernible *a priori*, exactly in which parameter-regime the symmetry will be broken at the “exceptional points” and further, the symmetry breaking is spontaneous [33]. Conservation of currents from a general field-theoretic perspective was established for the \mathcal{PT} operation by Alexandre et al. [34].

If it is required that the regions I through IV have \mathcal{PT} symmetry incorporated in the potential (energy) part, with the \mathcal{P} (parity) operation carried out around the median $y = b/2 \equiv b_2$, that is accomplished through $y - b/2 \rightarrow b/2 - y$. As is well-known, if the potential is completely real, \hat{H} is manifestly hermitian with no extra restrictions for reality of its associated eigenvalues. However, when a real potential in some sector is accompanied by a complex valued or a pure imaginary one in another sector, real eigenvalues in the sustained, unbroken \mathcal{PT} regime could result only when the $Re(V)$ is an even, i.e. a symmetric function under spatial inversion (parity), while the $Im(V)$ is odd, i.e. antisymmetric. We shall impose this requirement on the general, complex-valued potential distributions chosen herein.

For the rectangular 2D rigid box studied herein we set $a = \sqrt{3}, b = \sqrt{2}$ both in the units of Bohr radii. Such a choice of irrational distance units should keep the accidental degeneracies to the minimum, if not completely suppress them. Further, b_1 and b_3 , located symmetrically with respect to the median $b_2 = b/2$ are set to: $b_1 = 0.4b$ and $b_3 = 0.6b$.

3.1 Real valued striped potentials

Since, even the striped real valued 2D potential distribution seems to have eluded attention, for an initial orientation, we present seven representative sets of all completely real-valued potentials with qualitatively different choices for V_1, V_2, V_3, V_4 (in Rydberg energy units). The Hamiltonian operator on the left of Eq. (1) is manifestly hermitian for this case, with no further symmetry requirements. Table-I presents five lowest energy eigenvalues, of course all of them real, for each of the seven adumbrative cases (I-VII); while Figure-2 depicts the pertinent 2D probability densities $|\psi(x, y)|^2$, where the portrayals are individually normalized albeit drawn to arbitrary scales. Figure-2 succinctly conveys that the probability exhibits varying degrees of localization, region-wise. Hereafter, distances in multiples of Bohr radii and energy values in Rydberg units will be understood. The “Baseline” refers to the standard problem where the inside potential identically zero, and as is evident, for which the y -separation also occurs; so that with

$n_x^{(0)} = 1$, n_y also has a fixed value.

Table I: Some typical, all-real-valued, seven sets of “striped” potentials (i.e. potential energies, in Ry) along the four y -stripes (Figure-1) and the associated lowest five energy eigenvalues for a rectangular rigid box with x length $a = \sqrt{3}$ and y -width $b = \sqrt{2}$ in units of a_B , the Bohr radius. The parameter $n_x^{(0)} = 1$ so that the y -solution governs the number of peaks (cf. Eq.(6)). For comparison, the “Baseline” refers to the standard rigid box with the inside potential identically zero.

Set	Potentials in y -strips (Ry)				Lowest five energy eigenvalues (Ry)				
	V_1	V_2	V_3	V_4	E_1	E_2	E_3	E_4	E_5
Baseline	0	0	0	0	8.224	23.03	47.70	82.25	126.7
I	+100	-100	+100	-100	-72.61	-6.131	18.88	112.7	134.9
II	+100	-100	-100	+100	-43.67	83.23	130.1	145.2	203.8
III	-100	+100	+100	-100	-72.69	-72.22	-3.023	0.230	98.42
IV	+100	-100	+100	+100	12.56	119.9	132.9	171.9	211.8
V	-100	+100	-100	-100	-80.60	-72.45	-32.74	-1.211	46.75
VI	+100	-100	-100	-100	-85.05	-50.30	6.566	81.70	132.2
VII	-100	+100	+100	+100	-72.45	-1.436	101.7	121.6	161.1

The baseline energy levels are of course $E = E_{n_x, n_y}^{(0)} = \frac{\pi^2 \hbar^2}{2\mu} \left(\frac{n_x^2}{a^2} + \frac{n_y^2}{b^2} \right)$; presented in Table-I: $n_x = n_x^{(0)} = 1$ and n_y values sweep through 1, 2, 3, 4 and 5 where the baseline ground state ($n_x^{(0)} = 1, n_y = 1$) probability density displays a single, flat peak (Figure-2). Although we shall not present in detail here, the expansion coefficients turn out contributing significantly at best only for the n_y values ranging from $n_y \sim 1 - 8$.

3.2 Introducing \mathcal{PT} symmetric potentials

Next, we appraise the effect of introducing \mathcal{PT} symmetry in the striped regions. We shall consider only the cases with nontrivial scenarios, where the participant states in \mathcal{PT} sustenance and breakdown often will, but need not always imperatively involve, the ground-state. Unless otherwise specified, we employ the eigenvalue-labeling convention from MATHEMATICA [32] where magnitude-wise the largest eigenvalues are labeled in diminishing order of their magnitude. Labeling the energy-sequence “ p ” in this reverse order, \mathcal{PT} scenarios surrounding $p = 50, 49, 48, \dots$ will be considered.

Consider the case where the two outer stripes are held at zero potential ($V_1 = V_4 = 0$) while the inner two sectors are rendered \mathcal{PT} symmetric, choosing ($V_2 = i\lambda = V_3^*$) with the real, positive parameter λ being continuously varied over the range 0 through 100. Figure-3 plots the profiles for $Re(E_p)$ and $Im(E_p)$, respectively the real and imaginary-parts of the energy levels, for $p = 50$ as well as for $p = 49$ whose starting points happen to be truly the ground and the first excited states. Initially, \mathcal{PT} symmetry is retained as the two levels continue to remain conspicuously real valued and distinct, slowly start drifting

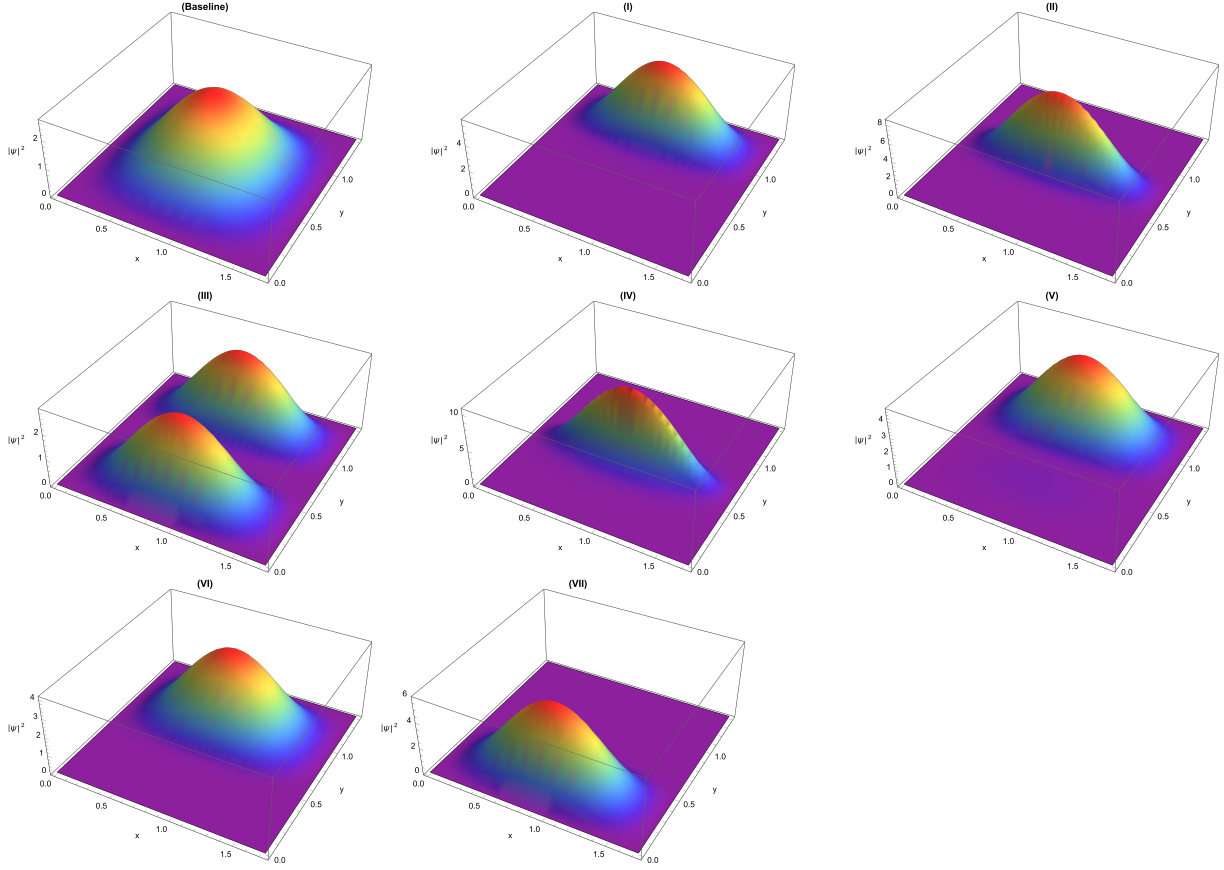


Figure 2: A collage of normalized ground states 2D probability densities $|\psi(x, y)|^2$ (plotted in arbitrary units), respectively corresponding to the seven sets of striped, all real potentials tabulated in Table-I for the corresponding ground states (panels I through VII). The familiar “Baseline” ($V = 0$ everywhere inside the box) Figure precedes the profiles I-VII, for comparison.

toward each other and merge together at a characteristic critical threshold value $\lambda_c = 54.5$, the exceptional ‘critical’ point, precisely at which the breakdown is triggered. For $\lambda > \lambda_c$, there is a complete \mathcal{PT} breakdown for the two energy levels E_{50} and E_{49} , which thereafter start occurring in complex conjugate pairs, in consonance with Eq.(11), as demarcated in Figure-3. In similar fashion, raising the potentials in the two y -borderline sectors by setting $V_1 = V_2 = 100$, and once again setting $V_2 = i\lambda = V_3^*$ sweeping the range $(0 - 100)$, the starting points here too happen to be exactly the ground and the first excited states, the exceptional point shifts upward to $\lambda_c = 84.0$, exhibiting higher degree of retention of \mathcal{PT} symmetry, as is evident from the transition depicted in Figure-4.

Next, we scrutinize the response to \mathcal{PT} symmetry by interchanging preceding two blocks: with now the outer sectors held non-hermitian \mathcal{PT} symmetric: $V_1 = i\lambda = V_4^*$ and $\lambda \rightarrow (0 - 100)$ while, the interior set to zero: $V_2 = 0 = V_3$ (the quantum number $n_x^{(0)} = 1$, as before). A remarkable \mathcal{PT} behavior then becomes manifest: First at the

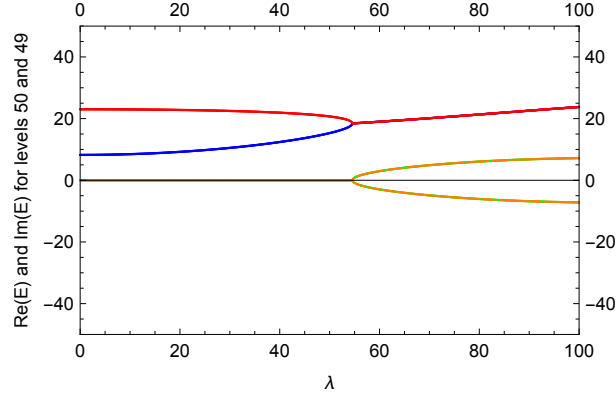


Figure 3: Plots for $Re(E_p)$ and $Im(E_p)$ parts of the eigenvalues E_p , versus the parameter λ in $V_2 = i\lambda = V_3^*$; $V_1 = 0 = V_4$ for the levels $p = 50$ and $p = 49$. Blue plot: $Re(E_{50})$, red plot: $Re(E_{49})$. \mathcal{PT} symmetry is retained, yielding real eigenvalues, up to the critical value $\lambda_c = 54.5$ (“exceptional point”) wherein the orange and green (overlapped) plots for $Im(E_{50})$ and $Im(E_{49})$ respectively, are zero up to λ_c beyond which the symmetry breaks down. Thereafter, the real parts merge together, while the imaginary parts are rendered equal and opposite, signifying occurrence of the eigenvalues in complex conjugate pairs. Energies in Ry, distances in Bohr radii. The quantum number $n_x^{(0)}$ has been clamped to unity.

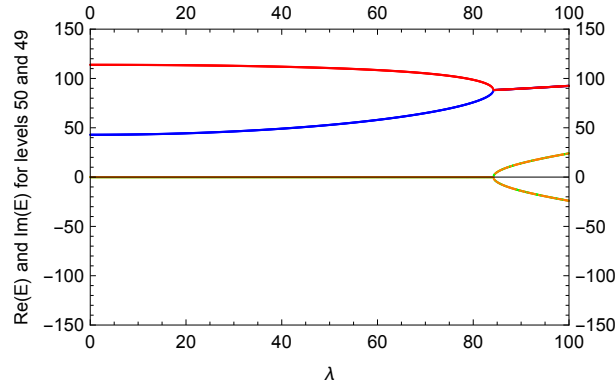


Figure 4: $V_2 = i\lambda = V_3^*$, $\lambda \rightarrow (0 - 100)$ and $n_x^{(0)} = 1$. The bordering sectors however are now held at a higher potential $V_1 = 100 = V_4$. $Re(E_p)$ and $Im(E_p)$ are plotted versus λ , blue plot: $Re(E_{50})$, red plot: $Re(E_{49})$. \mathcal{PT} breakdown occurs at a higher $\lambda_c = 84.0$. Likewise as in Figure-3, the orange and green (overlapped) plots represent $Im(E_{50})$ and $Im(E_{49})$. Again, beyond λ_c , the real parts merge and eigenvalues emerge only as complex conjugate pairs.

exceptional point $\lambda_{c_1} = 1$ (first criticality), a \mathcal{PT} breakdown occurs for the two lowest two levels $p = 50$ (ground-state for $\lambda = 0$), $p = 49$ (immediately succeeding excited state for $\lambda = 0$). Thereafter, instead of continuing with the symmetry breach throughout the remainder of the λ -range, a *second* criticality emanates for the level E_{50} at $\lambda_{c_2} = 51.0$, where, surprisingly, not only there is a complete *restoration* of \mathcal{PT} symmetry (i.e. being bestowed with completely real eigenvalues), for the (erstwhile-) lowest level E_{50} , but concomitantly, at precisely the same juncture, the next two higher states with $p = 49$ and 48 “collude” together triggering a \mathcal{PT} symmetry-breaking transition. Further, this ‘crossover’ is particularly a smooth one, i.e. with no sudden kinks, as is vividly purported by the collages of the plots in Figures-5 and 6. Note that at the point of second criticality λ_{c_2} , E_{50} abruptly jumps upward and smoothly continues the sojourn of the state

E_{48} , the latter steadily linking itself with the \mathcal{PT} breakdown curve but now by coupling with the state E_{49} , with $Re(E_{48})$, $Re(E_{49})$ congruently merging together. It is thus clear that, for real valued eigenvalues, unlike in adiabatic change of the parameters, the energy hierarchy is not necessarily preserved under \mathcal{PT} transitions. These counterintuitive tripartite peregrinations of the transiting participant states cannot be predicted *a priori*.

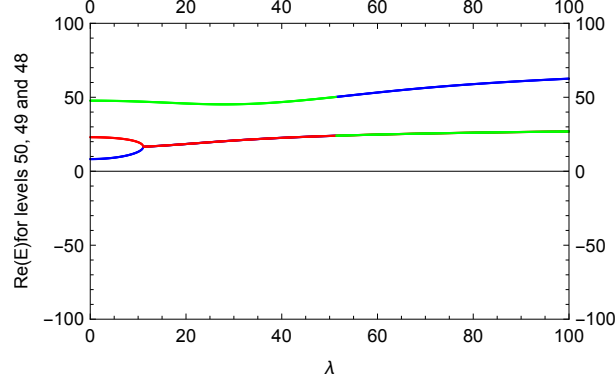


Figure 5: $Re(E_p)$ vs. λ behavior for $p = 50$ (blue), $p = 49$ (red) and $p = 48$ (green), with the outer sectors imparted \mathcal{PT} symmetric: $V_1 = i\lambda = V_4^*$; inside, $V_2 = 0 = V_3$. The range swept is: $\lambda \rightarrow (0 - 100)$. The quantum number $n_x^{(0)} = 1$, as before. A remarkable interplay of sustenance and breaking of \mathcal{PT} occurs: First breakdown for $p = 50, 49$ at $\lambda_{c_1} = 11.0$; \mathcal{PT} restoration for $p = 50$ and a ‘crossover’ leading to breaking for $p = 49$ and 48 , at $\lambda = 51.0$ is evident. See the text for fuller details; cf. also the next figure (Figure-6).

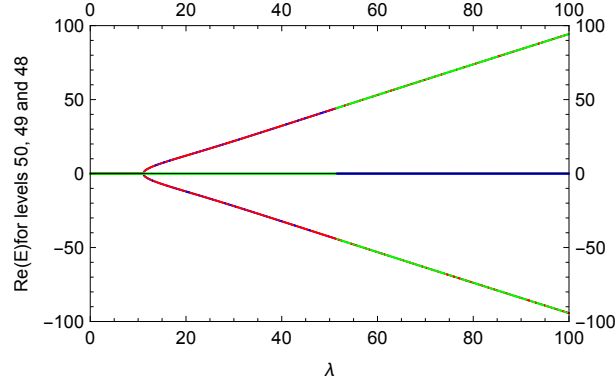


Figure 6: $Im(E_p)$ vs. λ behavior for $p = 50$ (blue), $p = 49$ (red) and $p = 48$ (green). The other control parameters are the same as those in Figure-5. On the extreme left, between the first ($\lambda_{c_1} = 11.0$) and the second ($\lambda_{c_2} = 51.0$) criticality, the blue and red plots perfectly overlap, giving a magenta type hue. Post λ_{c_2} , the eigenvalue E_{50} becomes completely real; concomitantly preceding two eigenvalues emerge with $E_{49} = E_{48}^*$, suffering a \mathcal{PT} breakdown.

Next, we empower the extreme two sectors with strong \mathcal{PT} symmetry, vide $V_1 = 50i = V_4^*$ and vary $V_2 = i\lambda = V_3^*$ with $\lambda \rightarrow (0 - 100)$ while, $n_x^{(0)}$ still kept locked at unity, thus all the four regions are made non-hermitian \mathcal{PT} symmetric. In response, \mathcal{PT} that is broken right in the beginning dismally fails to recover and continues to be breached, as the plots in Figure-7 elucidate.

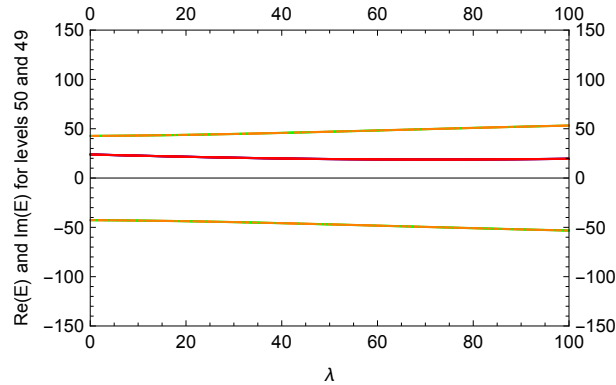


Figure 7: $Re(E_{50}) = Re(E_{49})$ (both completely merged, in red) and $Im(E_{50}) = -Im(E_{49})$ (orange-colored plots), for a strong, fixed choice of $V_1 = 50$ $i = V_4^*$ and varying $V_2 = i\lambda = V_3^*$ $\lambda \rightarrow (0 - 100)$. \mathcal{PT} breakdown, right from the start is evident throughout.

Incidentally, the present work turns out, in a sense, ‘a spatial counterpart’ to the interesting recent work by Hayrapetyan, Klevansky and Götte [35], who introduced in a spatially homogeneous optical medium, a time-dependent \mathcal{PT} symmetric dielectric permittivity and demonstrated within the framework of classical electrodynamics, the consequent light amplification as well as attenuation.

3.3 Probability density mutations

Probability redistributions surrounding some typical \mathcal{PT} transitions, are presented next. Absolute squared of the ground-level wave function $|\psi(x, y)|^2$, pre (left plot of Figure-8) and post(right plot of Figure-8) \mathcal{PT} breaking, presented to scale, reflects non-unitarity (in fact antiunitarity) of the composite \mathcal{PT} operation evidenced from attenuation in one of the peaks for the state E_{50} , after criticality ($\lambda_c = 55.4$), for the same parameters as in Figure-3.

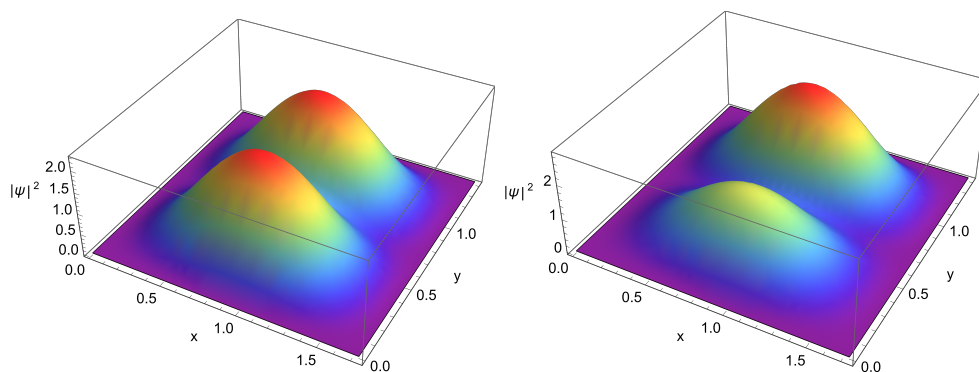


Figure 8: Pre (left) and Post (right) \mathcal{PT} breaking Probability density $|\psi(x, y)|^2$ for the ground-level E_{50} , with the same parameterization as in Figure-3; with $\lambda = 54 < 54.5 = \lambda_c$ for pre- \mathcal{PT} while, $\lambda = 56 > 54.5 = \lambda_c$ for post- \mathcal{PT} scenario.

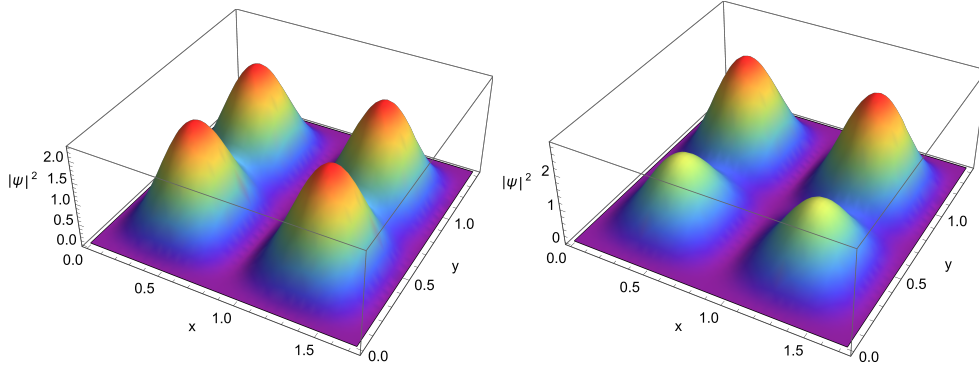


Figure 9: Pre (plot to the left) and Post (plot to the right) \mathcal{PT} breaking Probability density $|\psi(x,y)|^2$ for the ground-level E_{50} , $n_x^{(0)} = 2$ with otherwise the same parameterization as in Figure-3; with $\lambda = 54 < 54.5 = \lambda_c$ for pre- \mathcal{PT} and $\lambda = 56 > 54.5 = \lambda_c$ for post- \mathcal{PT} scenario.

Not surprisingly, this breakdown also prevails for $n_x^{(0)} = 2$ where both the peaks deteriorate (Figure-9); the factored out x -part of course having no direct role to play in the present \mathcal{PT} gamut.

Incidentally, with a small number of partitions as portrayed in Figure-1, it is straightforward to approach the present problem *directly*. In the respective regions, one has the following forms for the wave functions:

$$\begin{aligned}
 \psi(x,y) &\sim A \sin\left(\frac{n_x^{(0)}\pi x}{a}\right) \sin(k_1 y) ; && \text{Region-I} \\
 \psi(x,y) &\sim \sin\left(\frac{n_x^{(0)}\pi x}{a}\right) [B \sin(k_2 y) + C \cos(k_2 y)] ; && \text{Region-II} \\
 \psi(x,y) &\sim \sin\left(\frac{n_x^{(0)}\pi x}{a}\right) [F \sin(k_3 y) + G \cos(k_3 y)] ; && \text{Region-III} \\
 \psi(x,y) &\sim H \sin\left(\frac{n_x^{(0)}\pi x}{a}\right) \sin[k_4(y-b)] ; && \text{Region-IV} \quad (12)
 \end{aligned}$$

the constant coefficients determinable by matching only the y -factors of wave functions and their derivatives at the respective interfaces, with the constants $\{k_i\}_{i=1}^4$ prescribed by the connection

$$\frac{\hbar^2}{2\mu} k_i^2 = E - V_i + \frac{\pi^2 \hbar^2}{2\mu} \left(\frac{n_x^{(0)}}{a}\right)^2 ; \quad \forall i = 1, \dots, 4 \quad (13)$$

Note that the energy eigenvalues E are unknown to begin with; the task is then tantamount to solving for the eigenvalues and the wave functions, the latter through determination of the coefficients. However, this approach leads to a formidable set of coupled transcendental equations tractable only through numerical techniques; the situation getting increasingly aggravated as the number of partitions increases. Moreover, if one did venture to solve these simultaneously, one can in principle obtain but only a *specific* en-

ergy eigenvalue at a time. For instance, even in the completely Hermitian case (all real potentials) the energy hierarchy will be indiscernible under this direct approach, as it is unclear *a priori*, exactly which eigenvalue - ground or excited - has resulted. The present matrix approach, on the other hand offers a holistic method that unequivocally yields the complete eigenspectrum.

3.4 \mathcal{PT} symmetric electrostatic potential

\mathcal{PT} symmetry that hinges on an intricate balance between gain and loss mechanisms is also investigated furnishing a fictitious electric field with a backdrop of the striped box, for the particle moving in the box possessing an electric charge q . Consider a uniform electric field, say along the y -direction, $\vec{F} = F_o \hat{j}$ furnished inside the box, and zero outside. This engenders the electrostatic potential (energy), once again with a manifest explicit dependence only on the y -coordinate (apart from a trivial additive constant set to zero here): $V(x, y) \equiv V(y) = -\alpha(y - b/2)$ with $\alpha = qF_o$. A real α imparts reality to V , which is manifestly antisymmetric around $y = b/2$, but still rendering the Hamiltonian hermitian; whilst a pure imaginary $\alpha = i\lambda$, $\lambda \in \mathbb{R}$, generates a non-hermitian but a truly \mathcal{PT} symmetric Hamiltonian associated with the corresponding electric field. Following a similar chain of arguments as was done surrounding Eqs. (1) through (9) above for the striped potential distribution, the electric field gives rise to simple prescriptions for the corresponding M - matrix, M^{el} , as described below.

Since V corresponding to the electric field is clearly antisymmetric in the y -coordinate around the median, the pertinent integrals all vanish for diagonal part of M^{el} , resulting strikingly, in exactly the same contribution as that of the rigid box with identically zero inside potential,

$$M_{n'_y, n_y}^{el} = \frac{\pi^2 \hbar^2}{2\mu} \left[\frac{(n_x^{(0)})^2}{a^2} + \frac{(n_y)^2}{b^2} \right] \quad (14)$$

for the diagonal elements ($n'_y = n_y$), while the off-diagonal portion can be written as

$$M_{n'_y, n_y}^{el} = -\frac{\alpha b}{\pi^2} \left[\frac{1}{(n'_y + n_y)^2} - \frac{1}{(n'_y - n_y)^2} \right] (1 - (-1)^{n'_y + n_y}) \quad (15)$$

hence, contributing only for odd combinations of $n'_y + n_y$; vanishing otherwise.

If the electric field contribution is taken in conjunction with that of the striped potential, for the combined problem, only the off-diagonal part, Eq. (9), must simply be *augmented* by the expression on the right of Eq. (15) above. Of the number of qualitatively diverse combinations of the striped potential annexed by the uniform electric field,

we shall herein present only a couple of salient aspects, summarized in Figure-10. For a \mathcal{PT} Symmetric Electric Field borne by $\alpha = 20i$ along with a ‘moderate’ \mathcal{PT} symmetric backdrop of $V_1 = 5i = V_4^*$ and $V_2 = -5i = V_3^*$, \mathcal{PT} is preserved throughout (top panels, Figure-10) as the resulting energy levels are all real. Enhancing the background \mathcal{PT} strength with the choice $V_1 = 100i = V_4^*$ and $V_2 = -100i = V_3^*$ the symmetry, albeit preserved for the ground-level, does break off for a handful, though not exhaustively all, of the higher ones (bottom panels, Figure-10), with emergence of equal and opposite imaginary parts. The $Re(E)$ plots are similar but not identical and practically indistinguishable on the scale plotted. There thus are interesting trade-offs between \mathcal{PT} symmetry transitions caused by the fictitious electric field and of the striped potential.

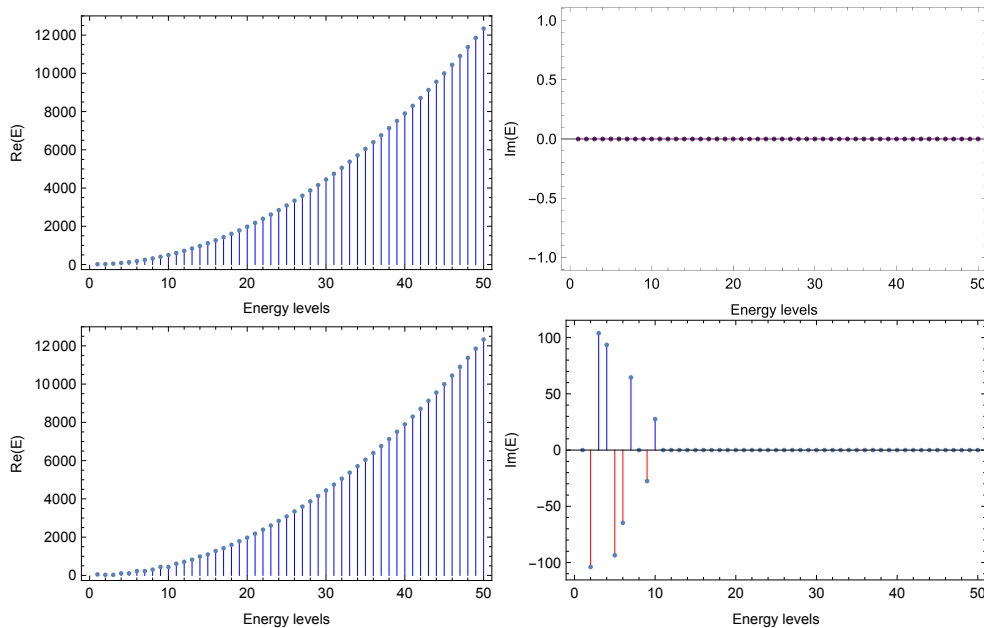


Figure 10: Top panels: The Real (Left) and Imaginary (Right) parts of the eigenenergies for a \mathcal{PT} symmetric Electric Field $\alpha = 20i$, with a \mathcal{PT} symmetric backdrop: $V_1 = 5i = V_4^*$ and $V_2 = -5i = V_3^*$. \mathcal{PT} is preserved throughout: the eigenvalues are all real. Bottom panels: $\alpha = 20i$, with a stronger \mathcal{PT} backdrop, $V_1 = 100i = V_4^*$ and $V_2 = -100i = V_3^*$, the symmetry breaks for a few states. For convenience and to guide the eye, the eigenvalues have been labeled from 1 through 50 in increasing order of their magnitude.

4 Conclusions

In summary, the present article derives exact quantum mechanical solutions for a 2D rectangular rigid box with a piecewise constant set of potentials in parallel, contiguously connected rectangular sectors or ‘stripes’ that have their widths the same as that of the box, forming a special type of quantum-billiards. These potentials are studied to gauge

the response of a scalar particle both under hermitian and non-hermitian yet \mathcal{PT} symmetric attributes ascribed, and combinations thereof. In the latter, several interesting \mathcal{PT} symmetry sustenance and breakdown transition scenarios emerge, including an intriguing reinstating of the broken symmetry for an energy level, concomitant with a smooth crossover of breakdown transition transferred to higher states. \mathcal{PT} symmetry that hinges on an intricate balance between gain and loss mechanisms is also investigated with a fictitious electric field furnished against a backdrop of the striped box. It is gratifying all that these spectacular systems are amenable to an exact quantum mechanical treatment. It would be instructive to investigate the temporal evolution of an initially localized wavepacket (with compact support) within the box, as well as under exotic electromagnetic fields, within the \mathcal{PT} symmetric framework. These studies are currently under investigation.

Acknowledgments

The authors are immensely indebted to Professor Dr. P. Durganandini for several interesting discussions on the current theme, and her encouragement throughout. SK is supported by University Grants Commission's Faculty Recharge Programme (UGC-FRP), Govt. of India, New Delhi, India.

References

- [1] S. W. McDonald and A. N. Kaufman, "Spectrum and Eigenfunctions for a Hamiltonian with Stochastic Trajectories, *Phys. Rev. Lett.* **42**, 1189 (1979).
- [2] For a lucid account, see S. R. Jain and R. Samajdar, "Nodal portraits of quantum billiards: Domains, lines, and statistics," *Rev. Mod. Phys.* **89**, 0450051 (2017). and references therein.
- [3] R. W. Robinett, "Visualizing classical periodic orbits from the quantum energy spectrum via the Fourier transform: Simple infinite well examples", *Am. J. Phys.* **65**, 1167 (1997).
- [4] R. W. Robinett, "Isolated versus nonisolated periodic orbits in variants of the two-dimensional square and circular billiards," *J. Math. Phys.* **40**, 101 (1999).
- [5] R. W. Robinett, "Quantum mechanics of the two-dimensional circular billiard plus baffle system and half-integral angular momentum," *Eur. J. Phys.* **24**, 231 (2003).

- [6] R. W. Robinett, “Energy Eigenvalues and Periodic Orbits for the Circular Disk or Annular Infinite well,” *Surface Review and Letters*, **5**, 519 (1998).
- [7] M. A. Doncheski, S. Heppelmann, R. W. Robinett, and D. C. Tussey, “Wave packet construction in two-dimensional quantum billiards: Blueprints for the square, equilateral triangle, and circular cases,” *Am. J. Phys.* **71**, 541 (2003).
- [8] M. A. Doncheski and R. W. Robinett, “Quantum Mechanical Analysis of the Equilateral Triangle Billiard: Periodic Orbit Theory and Wave Packet Revivals,” *Ann. Phys.* **299**, 208 (2002).
- [9] I. Kosztin and K. Schulten, “Boundary integral method for stationary states of two-dimensional quantum systems,” *Int. J. Mod. Phys. C* **08**, 293 (1997).
- [10] D. L. Kaufman, I. Kosztin, and K. Schulten, “Expansion method for stationary states of quantum billiards,” *Am. J. Phys.* **67**, 133 (1999).
- [11] P. J. Richens and M. V. Berry, “Pseudointegrable systems in classical and quantum mechanics,” *Physica 2 D*, **495** (1981).
- [12] M. J. Berry, J. A. Katine, R. M. Westervelt, and A. C. Gossard, “Influence of shape on electron transport in ballistic quantum dots,” *Phys. Rev. B (RC)* **50**, 17721 (1994).
- [13] S. Montangero, D. Frustaglia, T. Calarco, and R. Fazio, “Quantum billiards in optical lattices,” *Europhys. Lett.* **88**, 300061 (2009).
- [14] C. M. Bender and S. Boettcher, “Real Spectra in Non-Hermitian Hamiltonians Having PT Symmetry,” *Phys. Rev. Lett.* **80**, 5243 (1998).
- [15] For an excellent perspective, subtleties, rigorous analysis as well as a compendium on contemporary theoretical and experimental developments in PT Symmetry, see C. M. Bender, P. E. Dorey, C. Dunning, A. Fring, and D. W. Hook, “PT symmetry in Quantum and Classical Physics,” World Scientific, Hackensack, N.J. (2019).
- [16] For an excellent review of recent experimental advancements and future directions, see R. El-Ganainy, K. G. Makris, M. Khajavikhan, Z. H. Musslimani, S. Rotter, and D. N. Christodoulides, “Non-Hermitian physics and PT symmetry,” *Nature Physics* **14**, 11 (2017).

- [17] For a comprehensive review of theoretical and experimental developments, see “Springer Tracts in Modern Physics: Parity-time(PT) Symmetry and its Applications”, edited by D. Christodoulides and J. Yang, Springer Nature (Singapore, 2018).
- [18] S. Bittner, B. Dietz, U. Günther, H. L. Harney, M. Miski-Oglu, A. Richter, and F. Schäfer, “PT Symmetry and Spontaneous Symmetry Breaking in a Microwave Billiard,” *Phys. Rev. Lett.* **108**, 024101 (2012).
- [19] A. Dasarathy, J. P. Isaacson, K. Jones-Smith, J. Tabachnik, and H. Mathur, “Particle in a box in PT-symmetric quantum mechanics and an electromagnetic analog,” *Phys. Rev. A* **87**, 062111 (2013).
- [20] Z. Gu, N. Zhang, Q. L. M. Li, S. Xiao, and Q. Song, “Experimental demonstration of PT -symmetric stripe lasers” *Laser Photonics Rev.* **10**, 588 (2016).
- [21] M. Kreibich, “Realizations of PT–symmetric Bose-Einstein Condensates with Time-dependent Hermitian Potentials,” Doctoral Dissertation, Institut für Theoretische Physik der Universität Stuttgart (2015).
- [22] Z. H. Musslimani, K. G. Makris, R. El-Ganainy, and D. N. Christodoulides “Optical Solitons in PT Periodic Potentials,” *Phys. Rev. Lett.* **100**, 030402 (2008).
- [23] J. Yusupov, S. Rakhmanov, D. U. Matrasulov, and H. Susanto, “Quantum dynamics of PT–symmetrically kicked particle confined in a 1D box,” *J. Phys. A: Math. Theor.* **52**, 055303 (2019).
- [24] S.B. Adamu, “Quantum Particle in a PT -symmetric Well,” M.Sc. Dissertation, Eastern Mediterranean University, Cyprus (2014).
- [25] F. M. Fernández and J. Garcia, “Parity-time symmetry broken by point-group symmetry,” *J. Math. Phys.* **55**, 042107 (2014).
- [26] K. S. Agarwal, R. K. Pathak, and Y. N. Joglekar “Exactly solvable PT -symmetric models in two dimensions,” *Europhys. Lett.* **112** , 31003 (2015).
- [27] K. S. Agarwal, R. K. Pathak, and Y. N. Joglekar, “Raising the PT -transition threshold by strong coupling to neutral chains,” *Phys. Rev. A* **97**, 042107 (2018).
- [28] P. Cherian, K. Abhinav, and P. K. Panigrahi, “From particle in a box to PT-symmetric systems via isospectral deformation,” (ongoing) [[arXiv:1110.3708v4](https://arxiv.org/abs/1110.3708v4) [math-ph]] (2013).

- [29] S. Klaiman, U. Günther, and N. Moiseyev, “Visualization of Branch Points in PT-Symmetric Waveguides,” *Phys. Rev. Lett.* **101**, 08402 (2008).
- [30] J.D. Bjorken and S. Drell, “Relativistic Quantum Mechanics,” McGraw-Hill, New York (1964), Section 5.4, Eq. (5.14), pp. 73.
- [31] J. J. Sakurai and J. J. Napolitano, “Modern Quantum Mechanics”, Second Edition, Addison-Wesley, Boston, MA (1994): Chapter 4, Section 4.4, Eq. (4.4.60), pp.294.
- [32] S. Wolfram, “The MATHEMATICA Book,” Fifth Edition, Wolfram Media Champaign, IL, USA (2003): Section 3.7.9, pp.17.
- [33] C. M. Bender, “The complex pendulum,” *Phys. Rep.* **315**, 27 (1999).
- [34] J. Alexandre, P. Millington, and D. Seynaeve, “Symmetries and conservation laws in non-Hermitian field theories,” *Phys. Rev. D* **96**, 065027 (2017).
- [35] A.G. Hayrapetyan, S. P. Klevansky, and J. B. Götte, “Instantaneous modulations in time-varying optical potentials.”, *New J. of Physics* **19**, 105002 (2017).